Energy-Efficient Thermal Management of Periodic Electronic Cavities Using the Cascaded Lattice Boltzmann Method: Optimization of the Air Inlet Inclination

Fatima Zahra LAKTAOUI AMINE[1*], *Mariam* JADAL[2], *Mohamed* ERREBII[1], *Abdeslem* Dhilou[1], *Abdelhakim* ANFLOUS[1], *Mohamed* RHOUZALI[3], *Mustapha* EL ALAMI[1], and *Elalami* SEMMA[4]

[1]LPMAT, Physics department, Faculty of Sciences Ain Chok, Hassan II University of Casablanca 20100, Casablanca, Morocco.
[2]LERMA, College of Engineering and Architecture, International University of Rabat, Parc Technopolis, Rocade de Rabat-Sale, Sala Al Jadida 11100, Morocco.
[3]LGITIL, Physics department, Faculty of Sciences Ain Chok, Hassan II University of Casablanca 20100, Casablanca, Morocco.
[4]L2ISA, Hassan First University, Settat 26000, Morocco.

Abstract. Efficient thermal management remains a major challenge in compact electronic systems, where increasing power density and confined geometries exacerbate heat accumulation and non-uniform temperature fields. This study proposes a geometry-driven optimization strategy based on the Cascaded Lattice Boltzmann Method (CLBM) to investigate mixed convection in a periodic cavity equipped with two heat sinks and inclined air inlets. The influence of the inlet inclination angle (φ=0°–80°) is systematically analyzed for fixed parameters K=50%, Ra=5×10^6, Pr=0.71, and Re=700. Numerical results reveal that the inlet inclination strongly governs the flow topology and the associated heat transfer mechanisms. At the optimal configuration, φ=45°, the formation of dual convection cells above the heat sinks promotes effective air recirculation and uniform cooling across all active surfaces. Compared with the baseline case (φ=0°), the thermal performance exhibits substantial gains: +14% in global Nusselt number, +13.58% on the vertical wall, +17.20% on the horizontal surface, and +23.60% within the micro-cavity. These improvements reflect a significant reduction in thermal resistance and enhancement of cooling uniformity, directly contributing to energy efficiency, component reliability, and extended device lifespan. Overall, this work highlights the potential of inlet-angle optimization as a simple yet powerful geometric control strategy for achieving high-performance and energy-efficient cooling in next-generation electronic enclosures.

Keywords: Mixed convection; Electronic cooling; Air Inlet inclination; CLBM; Energy-efficient thermal management; Periodic cavity.

* Corresponding author: laktaouiamine.fatimazahra@gmail.com

Nomenclature

C	Speed [m/s]
C_I	Propagation speed [m/s]
C_s	Sound speed [m/s]
D	Dimension (LBM)
dx_j	The differential along the wall
e_i	particle velocity [m/s]
F	External forces [N]
F_v	Body force [N]
f	Distribution function
f_i	Distribution function for a set of particles
f_i^{eq}	Equilibrium distribution function
g	Gravity acceleration [m/s^2]
g_i	Energy distribution function
g_i^{eq}	Equilibrium energy distribution function
H	Dimensionless height of the cavity
H_i	The height or width of the wall i
h	Dimensionless height of the heat sinks
K	Aspect ratio of the heat sinks
K_{mn}	Equilibrium values
IT	Iteration Number
L	Dimensionless length of the cavity
l	Dimensionless width of the cavity
n	Mesh
n_i	Normal on the wall
Nu	Local Nusselt number
Nu_g	Global Nusselt number

Nu_{g}^{m}	Global Average Nusselt number
$\boldsymbol{Nu_{g-in}^{m}}$	Global Average Nusselt number inlet side
$\boldsymbol{Nu_{g-h}^{m}}$	Global Average Nusselt number horizontal side
$\boldsymbol{Nu_{g-m-c}^{m}}$	Global Average Nusselt number micro-cavity side
$Nu_{R-\mathrm{R}}$	Number of Nusselt on the right-hand side heat sink right
Nu_{R-l}	Number of Nusselt on the right-hand side heat sink left
Nu_{l-R}	Number of Nusselt on the left-hand side heat sink right
Nu_{l-l}	Number of Nusselt on the left-hand side heat sink left
Nu_{h-R}	Number of Nusselt of the source horizontal heat sink right
Nu_{h-l}	Number of Nusselt of the source horizontal heat sink left
p	Dimensionless static pressure
P_r	Prandtl number
Q	Direction (LBM)
R_a	Rayleigh number ($Ra = \frac{g\beta\Delta TH^3}{\alpha\nu}$)
R_e	Reynolds number ($Re = \frac{V_0 H}{\nu}$)
S	Source term
T	Fluid temperature [°C]
T_0	Reference temperature [°C]
T_h	Hot temperature [°C]
T_c	Cold temperature [°C]
U	Dimensionless speed on ox
V	Dimensionless speed on oy
Γ	Moment [N.m]
θ	Dimensionless temperature ($\theta = \frac{T-T_c}{T_h-T_c}$)

α	Thermal diffusivity $[\frac{m^2}{s}]$
β	Expansion coefficient $[K^{-1}]$
ρ	Density $[\frac{kg}{m^3}]$
φ	Air jet inclination angle
ϑ	kinematic viscosity $[\frac{m^2}{s}]$
λ	Thermal conductivity [W/m. K]
ε	Relaxation factor
δt	Time variation [s]
τ	Dimensionless time

1 Introduction

Thermal management of electronic components is increasingly challenging as devices continue to shrink while power densities rise. The resulting thermal loads threaten system reliability, performance, and lifespan, making precise temperature control essential to avoid overheating-induced failures. Depending on application constraints, natural, forced, and mixed convection are commonly employed, with mixed convection combining buoyancy-driven flow and externally induced airflow offering an effective compromise that boosts heat transfer while limiting energy consumption, especially in space-constrained devices with controllable airflow. Numerical modeling is central to analyzing and optimizing the coupled thermo-fluid behavior in such coolers. In this context, the Cascaded Lattice Boltzmann Method (CLBM) has emerged as a robust, versatile approach for simulating flow and thermal convection; its capacity to accommodate complex geometries and faithfully capture fluid–thermal interactions make it particularly well suited for studying heat transfer within electronic cavities.

Meskini et al. [1] conducted a numerical simulation of mixed convection within a square cavity containing heated rectangular blocks exposed to a vertical air jet. The influence of Reynolds and Rayleigh numbers on flow topology and heat transfer was analyzed. The results revealed that stronger forced flow promotes cooling uniformity, whereas buoyancy effects introduce asymmetry and generate secondary vortices. Increasing the Reynolds number reduces temperature gradients and enhances the overall Nusselt number. The study highlighted the strong coupling between forced convection and block-induced recirculations in confined geometries.

Najam et al. [2] carried out a numerical analysis of unsteady mixed convection in a horizontal channel featuring periodically arranged heated blocks along the lower wall. The study explored the interplay between buoyancy and forced convection through examinations of the velocity field, temperature distribution, and Nusselt number variations. The findings indicated that increasing the Rayleigh number intensifies thermal instabilities and promotes recirculating zones, whereas higher Reynolds numbers stabilize the flow and enhance heat

transfer uniformity. The periodic configuration of the blocks was shown to play a crucial role in shaping boundary-layer development and improving overall cooling performance.

Closely related to the present study, Faraji et al. [3] used the Lattice Boltzmann Method (LBM) to investigate natural convection in air-filled heat sinks with multiple protrusions, emphasizing the strong impact of the Rayleigh number and enclosure inclination on thermal behavior. More recently, Mlikhi et al. [4] examined mixed convection of a magnetic nanofluid in a double-lid-driven convergent cavity, offering valuable insights into the optimization of thermal management strategies for electronic cooling applications.

Recent studies by Hidki et al. [5] and Ma et al. [6] have shown that employing hybrid nanofluids and introducing heated obstacles can markedly enhance heat transfer. Building on this, Selimefendigil and Öztop [7] examined how obstacle geometry, applied magnetic fields, and internal heat generation jointly affect convective transport and entropy production. Complementary investigations by Gawas and Patil [8] and Farahani et al. [9] demonstrated that cavity inclination and oscillating cylinders reshape flow structures in ways that significantly influence thermal performance.

Building on these findings, Das et al. [10] highlighted the pronounced impact of non-square enclosure geometries on convection behavior, offering valuable guidance for the design and optimization of more efficient thermal management systems.

The present study investigates a periodic rectangular cavity containing two heated heat sinks mounted on the bottom wall. Fresh air is injected through inclined side openings located adjacent to each heat sink, while the configuration is treated as periodic in the horizontal direction to represent a continuous array of identical cooling modules.

The objective is to analyze the effect of the air inlet inclination angle ($\varphi = 0° - 80°$) on the mixed convection behavior within the cavity. The simulations are carried out for a fixed heat sink height ratio $K = h/H = 50\%$, Rayleigh number $Ra = 5 \times 10^6$, Prandtl number $Pr = 0.71$, and inlet Reynolds number $Re = 650$. These conditions correspond to a transitional mixed convection regime, where forced flow and buoyancy interact strongly. By examining velocity field, temperature fields, and heat transfer (Nusselt number distributions), the study aims to determine the optimal inclination angle that maximizes cooling performance and ensures uniform thermal distribution within the periodically ventilated cavity.

This study utilizes the Cascaded Lattice Boltzmann Method (CLBM) to accurately resolve the complex interaction between mixed convection flow dynamics and heat transfer phenomena.

This work provides new insights into how airflow orientation governs the balance between buoyancy and forced convection effects. The use of the Cascaded Lattice Boltzmann Method (CLBM) enables high-fidelity resolution of complex flow–thermal interactions within a periodic cavity configuration, representative of real electronic module arrangements. The findings contribute to the optimization of passive–active hybrid cooling strategies, offering practical guidance for the design of compact, energy-efficient thermal management systems in next-generation electronic and data-center applications.

2 Physical and Mathematical Model

Effective thermal management of electronic components in compact enclosures is essential for reliable operation and extended service life, especially in high-power-density applications such as servers, automotive and aerospace ECUs, UPS modules, and GPU clusters. To represent these practical environments, the present configuration is a rectangular cavity of height $H$and length $1.18H$, containing two identical heat sinks mounted on the bottom wall. Each heat sink has a width of $0.17H$and a height ratio $K = h/H = 50\%$; its hot surface is maintained at temperature $T_{h,}$ representing scenarios ranging from low to very high-power densities. Laterally inclined air inlets of width $0.12H$are positioned adjacent to

each heat sink to inject fresh cooling air at temperature T_c, while the heated air exits through a top outlet of length $L' = 26H$. To assess the influence of flow direction, the inlet inclination angle φ varies from 0°to 80° (i.e., 0°, 30°, 45°, 60°, 70°, and 80°). Figure 1 illustrates the configurations Under study.

Periodic boundary conditions are imposed on the cavity's vertical sidewalls to emulate an infinitely repeating array of electronic modules. In this formulation, the flow and temperature fields are periodic in the horizontal direction, whereas the hardware layout (heat sinks and inlets/outlets) is not explicitly replicated beyond the computational cell. This periodic-cell approach captures lateral thermal interactions and local cooling behavior with high fidelity, while offering an efficient compromise between physical realism and computational cost.

The main objective of this study is to determine the optimal inlet inclination angle (φ) that maximizes cooling efficiency, minimizes thermal stratification, and ensures uniform heat removal from active surfaces, thereby providing practical design guidelines for compact and energy-efficient electronic cooling systems.

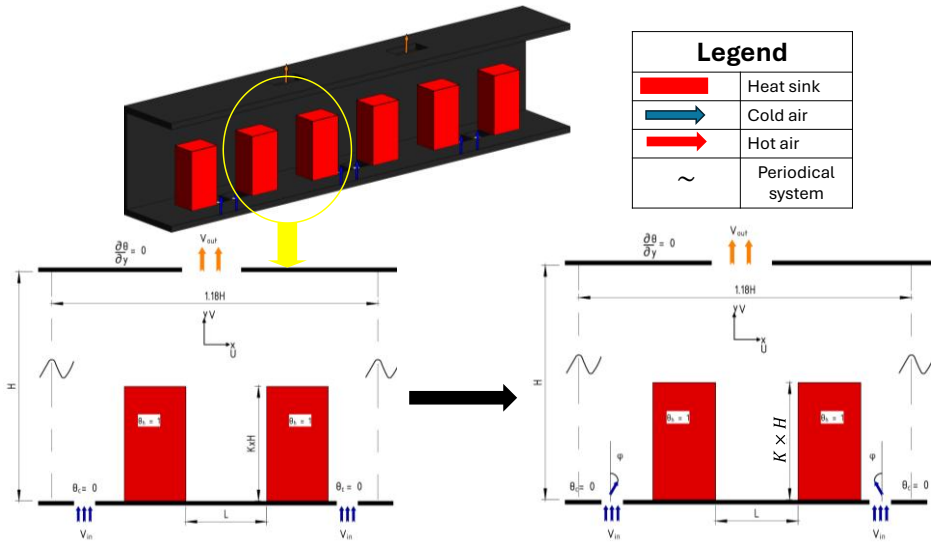

Fig. 1. Schematic representation of the investigated configuration

The following are the flow fields' macroscopic governing equations:

$$\nabla . u = 0 \tag{1}$$

$$\frac{\partial u}{\partial t} + (u.\nabla)\, u = -\frac{1}{\rho_0}.\nabla p + v\nabla^2 u + F \tag{2}$$

where F, v, u, p, $\boldsymbol{\rho}_0$ are the force field, kinematic viscosity, velocity, pressure, and reference density, in that order. The energy conservation equation is expressed as:

$$\frac{\partial T}{\partial t} + u.\nabla.T = \nabla.(\alpha.\nabla T) + S_T \tag{3}$$

The scalar variable and diffusion coefficient for the incompressible thermal flows considered in this work are given as temperature T and thermal diffusivity α, respectively. Bossiness assumption is used to include the impact of the temperature field on the flow field. The force field is defined as follows:

$$F = -g\beta\,(T - T_0)\,j + F_v \tag{4}$$

where T_0 is the reference temperature, j is the unit vector in the vertical direction, g is the gravitational acceleration magnitude, $\boldsymbol{F}_v$ is an external body force, and β is the thermal expansion coefficient.

The initial and boundary conditions associated with the problem under study are as follows:

- Initial conditions:

$$U\,(x,y) = V\,(x,y) = 0$$

On the heat sinks $\theta_h = 1$

On the rest of the cavity $\theta = 0$

- Dynamic and thermal boundary conditions:

No-slip boundary condition at the walls, $U = V = 0$

On supply openings $U = U_{jet} \times \sin(\varphi)\,, V = V_{jet} \times \cos(\varphi)$

On heat sinks $\theta_h = 1$

Dynamic boundary conditions are periodic on left-right odds

On supply openings $\theta_C = 0$

Outlet opening $\frac{\partial^2\theta}{\partial y^2} = 0, \frac{\partial^2 V}{\partial y^2} = 0\,,\, U = 0$

On the adiabatic plates $\frac{\partial\theta}{\partial n} = 0$

2.1 Cascaded Lattice Boltzmann Method (CLBM)

This study employs the Cascaded Lattice Boltzmann Method (CLBM) to model both flow and temperature fields. The detailed formulation of the CLBM method is not presented here and can be found in [11]. To simulate the flow and heat transfer within the cavity, the $D2Q9$ lattice structure is used. This model, which defines fluid motion over nine discrete velocity directions in a two-dimensional space, offers a good balance between computational simplicity and physical realism. It is particularly well suited for problems involving laminar, incompressible flows such as mixed convection, where both forced airflow and buoyancy effects are present. The $D2Q9$ scheme has become standard in thermal simulations due to its proven accuracy in capturing flow structures and temperature fields, especially in geometries like rectangular cavities. Its compatibility with boundary conditions commonly used in electronic cooling applications makes it a natural and efficient choice for the present study.

2.1.1 CLBM for the flow field

In this study, a two-dimensional (2D) problem is modeled using the Cascaded Lattice Boltzmann Method (CLBM). For the flow field, the standard D2Q9 lattice is used with normalized lattice speed $C = \frac{\Delta x}{\Delta t} = 1$. The discrete velocity vectors are $\boldsymbol{e_i} = [|e_{ix}>.|e_{iy}>]$

$$|e_{ix}> = [0,1,0,-1,0,1,-1,-1,1]^{\boldsymbol{T}} \tag{5a}$$

$$|e_{iy}> = [0,0,1,0,-1,1,1,-1,-1]^{\boldsymbol{T}} \tag{5b}$$

Where: i = 0 ... 8, $|.>$ .and denotes matrix transposition.

To construct the collision operator based on central moments, both raw moments K_{mn} and central moments $\bar{K}_{mn}$ are introduced:

$$K_{mn} = \langle f_i | e_{ix}^m e_{iy}^n \rangle \tag{6a}$$

$$\bar{K}_{mn} = \langle f_i | (e_{ix} - u_x)^m (e_{iy} - u_y)^n \rangle \tag{6b}$$

Equilibrium moments k_{mn}^{eq} and $\tilde{k}_{mn}^{es}$ are derived from the equilibrium distribution functions f_i^{eq}.

In this study, a simplified set of raw moments is used to reduce computational complexity:

$$|\Gamma_i> = [K_{00}, K_{10}, K_{01}, K_{20}, K_{02}, K_{11}, K_{21}, K_{12}, K_{22}]^{\boldsymbol{T}} \tag{7}$$

These are obtained from f_i using a transformation matrix **M,** and then converted into central moments using a shift matrix **N**:

$$|\Gamma_i> = \mathbf{M}|f_i> \tag{8}$$

$$\left|\bar{\Gamma}_I\right> = \mathbf{N}|f_i> \tag{9}$$

The collision step is performed by relaxing each central moment to its equilibrium value:

$$\left|\bar{\Gamma}_i^*\right> = (\boldsymbol{I} - \boldsymbol{S})\left|\bar{\Gamma}_i\right> + \boldsymbol{S}\left|\bar{\Gamma}_i^{eq}\right> + (\boldsymbol{I} - \frac{\boldsymbol{S}}{2})|C_i> \tag{10}$$

where C_i represents the source term vector and $\boldsymbol{S}$ is a diagonal matrix of relaxation rates. The equilibrium moments are based on the continuous Maxwell-Boltzmann distribution:
The equilibrium distribution function is given by:

$$f_i^{eq} = \rho\omega_i \left(1 + \frac{u.C_i}{C_s^2} + \frac{(u.C_i)^2}{2C_s^4} - \frac{u.u}{2C_s^2}\right) \tag{11}$$

where ρ is the density and $C_s = \sqrt{1/3}$ is the lattice sound speed.

The forcing term in velocity space is:

$$R_i = \frac{\boldsymbol{F}}{\rho}\frac{(\boldsymbol{e_i} - \boldsymbol{u})}{C_s^2} f_i^{eq} \tag{12}$$

And its central moment form:

$$|C_i> = \boldsymbol{NM}|R_i> = [0, F_x, F_y, 0,0,0, C_s^2 F_y, C_S^2 F_x, 0] \tag{13}$$

The streaming step is:

$$f_i = (\boldsymbol{X} + \boldsymbol{e_i}.\Delta t + \Delta t) = f_i^*(\boldsymbol{X}, t) \tag{14}$$

Where $|f_i^*> = \boldsymbol{M}^{-1}\boldsymbol{N}^{-1}\left|\bar{\Gamma}_i^*\right>$. The macroscopic variables are obtained by:

$$\rho = \sum_{i=0}^{8} f_i, \rho\boldsymbol{u} = \sum_{i=0}^{8} f_i \boldsymbol{e}_i + \Delta t\boldsymbol{F}/2 \tag{15}$$

An incompressible approximation is employed: $\rho = \rho_0 + \delta\rho$ Using Chapman-Enskog expansion, the incompressible Navier-Stokes equations are recovered with viscosities:

$$v = \left(\frac{1}{s_v} - 0.5\right) C_s^2 \Delta t, \varepsilon = (\frac{1}{s_b} - 0.5) C_s^2 \Delta t. \tag{16}$$

2.1.2. CLBM for the Thermal field

A D2Q5 lattice is used to solve the convection-diffusion equation for temperature. Moments of the temperature distribution function g_i are:

$$K_{mn}^T = \langle g_i | e_{ix}^m e_{iy}^n \rangle \tag{17a}$$

$$\bar{K}_{mn}^{T} = \langle g_i | (e_{ix} - u_x)^m (e_{iu} - u_y)^n \rangle \quad (17b)$$

The simplified moment set used is:

$$|\Gamma_i^T >= [k_{00}^T, K_{10}^T, K_{01}^T, K_{20+02}^T, K_{02-20}^T]^T \quad (18)$$

These are calculated using transformation and shift matrices $\boldsymbol{M_T}$ and $\boldsymbol{N_T}$

$$|\Gamma_i^T >= \boldsymbol{M_T}|g_i >, \ \left|\bar{\Gamma}_i^T\right. >= \boldsymbol{N_T}|\Gamma_i^T > \quad (19)$$

The collision step is:

$$\left|\bar{\Gamma}_i^{T,*}\right. >= (\boldsymbol{I} - \boldsymbol{S}_T)\left|\bar{\Gamma}_i^T\right. > + \boldsymbol{S}_T\left|\Gamma_i^{T,eq}\right. > \quad (20)$$

With $\boldsymbol{s}^T = d(\lambda_0, \lambda_1, \lambda_1, \lambda_2, \lambda_2)$.

The temperature equilibrium distribution is based on the Maxwell-Boltzmann form:

$$g^{eq} = \frac{T}{2\pi C_T^2} e^{-\frac{(\xi - \boldsymbol{u})^2}{2C_T^2}} \quad (21)$$

Equating discrete and continuous central moments yields:

$$\left|\bar{\Gamma}_i^{T,eq}\right. >= [T, 0, 0, Tc_T^2, Tc_T^2]^T \quad (22)$$

The post-collision distribution and streaming step:

$$g_i(\boldsymbol{X} + \boldsymbol{e}_i, t + \Delta T) = g_i^*(\boldsymbol{X}, t) \quad (23)$$

Temperature is then computed as:

$$T = \sum_{i=0}^{4} g_i \quad (24)$$

2.2 Nusselt Numbers

The efficiency of heat removal from the heat-generating components is assessed through the global average Nusselt number (Nu_g), which quantifies the overall convective heat transfer performance of the system.

The overall Nusselt number accounting for all the heated surfaces is then expressed as:

$$\boldsymbol{Nu_g} = \boldsymbol{Nu_{R-R}} + \boldsymbol{Nu_{R-l}} + \boldsymbol{Nu_{l-R}} + \boldsymbol{Nu_{l-l}} + \boldsymbol{Nu_{h-R}} + \boldsymbol{Nu_{h-l}} \quad (25)$$

The surface convective heat flux is also determined along each wall of the heat sources using the following relation:

$$Nu_i = \frac{1}{H_i}\int_0^{H_i} \frac{\partial \theta}{\partial x_j} dx_i \quad (26)$$

2.3 Mesh Independence Study and Numerical Code Validation

2.3.1 Mesh Independence Study

A mesh independence analysis was carried out to ensure that the numerical results are unaffected by grid refinement. Five uniform meshes ranging from 254×192 to 454×392 nodes were tested under identical conditions (φ=0◦, K=50%, Ra=5×10^6, Pr=0.71, Re=650). The global average Nusselt

number (Nu_{gm})and the maximum Stream function (Ψ_{max}) were used as primary indicators of numerical convergence. As shown in Table 1, Nu_{gm} increases from 35.10 on the coarsest grid to 37.54 on the finest one, while Ψ_{max} varies only slightly from 2.84 to 2.92.

The relative deviations between the two finest grids (404×342 and 454×392) are 0.19 % for Nu_{gm} and 0.34 % for Ψ_{max}, indicating that the solution has reached grid-independent behavior. Therefore, the mesh 404×342 was selected for all subsequent simulations as it provides an excellent compromise between numerical accuracy and computational efficiency. **Table.1**: Grid Independence Test for the Global Nusselt Number and Maximum Stream Function (K = 50%, $\varphi = 0°$).

Table 1. Mesh Sensitivity Analysis

Mesh	**254 × 192**	**304 × 242**	**354 × 292**	**404 × 342**	**454 × 392**
$\boldsymbol{Nu^m_g(\varphi = 0)}$	35.10	36.33	37.07	37.47	37.54
Deviation $\boldsymbol{Nu^m_g}$ (%)	-	3.50	2.04	1.08	0.19
$\boldsymbol{\Psi_{max}}$	2.84	2.87	2.89	2.91	2.92
Deviation $\boldsymbol{\Psi_{max}}$ (%)	-	1.06	0.70	0.69	0.34

2.3.2 Numerical Code Validation

To ensure the accuracy of the developed numerical model, both thermal and hydrodynamic validations were carried out. Table 2 presents a comparison of the dimensionless stream function maxima (Ψ_{max}) and global Nusselt number for the same Rayleigh numbers. Again, a close match is observed with reference solutions, with discrepancies remaining under 1.5%.

These validations demonstrate the robustness and accuracy of the numerical approach and establish a strong foundation for applying the model to the more complex mixed convection problem addressed in this study.

In addition to these benchmark-based validations, an experimental validation of the proposed CLBM framework has been reported in our previous work and can be found in Ref. [11,12].

Table. 2 Comparison maximum dimensionless streaming and Global Nusselt Number

$\boldsymbol{Ra}$	Present Results	De Vahl Davis [12]	Deviation %
$\mathbf{10^3}$	$Nu = 1.200$	$Nu = 1.181$	1.500
	$\Psi_{max} = 1.173$	$\Psi_{max} = 1.174$	0.085
$\mathbf{10^5}$	$Nu = 4.530$	$Nu = 4.503$	0.600
	$\Psi_{max} = 9.590$	$\Psi_{max} = 9.667$	0.796
$\mathbf{10^6}$	$Nu = 8.780$	$Nu = 8.800$	0.227
	$\Psi_{max} = 16.810$	$\Psi_{max} = 16.960$	0.884

3 Results and discussion

To evaluate the effect of inlet inclination, this section presents a detailed geometric analysis of the configuration. Simulations are performed under identical thermal conditions ($Ra = 5 \times 10^6$, $\mathrm{Pr} = 0.71$) with a fixed heat-sink aspect ratio $K = 50\%$, while the inlet angle $\varphi$is varied systematically. The response is examined qualitatively via streamlines and isotherms and quantitatively, using global and wall-resolved (local) average Nusselt numbers. This multi-level analysis clarifies the mechanisms underlying the observed thermal behavior and identifies inlet orientations that achieve targeted, uniform, and efficient cooling in compact electronic enclosures.

3.1 *Overall Behavior of Temperature Contours and Flow Patterns*

Figure 2 illustrates the streamline patterns for $K = 50\%$, where two heat sinks are placed between inclined lateral inlets. The inlet inclination angle φ plays a crucial role in defining how the air jets interact with the inlet-facing vertical walls, the top horizontal surfaces of the heat sinks, and the inter-block micro-cavity.

For $\varphi = 0°$, the air enters vertically and impinges directly on the bottom wall before rising along the inlet-facing surfaces. These vertical walls are therefore well ventilated, as the jet maintains close contact with them under the combined effects of forced convection and buoyancy. Conversely, the micro-cavity side remains poorly ventilated, where the air becomes almost stagnant, leading to weak convective heat removal and localized temperature accumulation.

When $\varphi = 30°$, the air jet begins to tilt, allowing a better interaction with the vertical inlet-facing walls. This inclination generates small recirculating cells in the upper corners of the cavity, which enhance mixing and redistribute thermal energy. However, the airflow penetration into the micro-cavity remains limited, and the overall flow pattern is still slightly asymmetric.

Under $\varphi = 45°$, the flow structure reaches its most balanced configuration. The inclined jet successfully interacts with all critical surfaces the vertical walls, the horizontal tops of the heat sinks, and the micro-cavity region. Two convection cells form above the heat sinks, forcing the cool air to circulate more extensively along the horizontal surfaces, which strengthens heat extraction and improves overall cooling uniformity. The resulting dual recirculation enhances the mixing intensity, leading to a more homogeneous thermal field within the cavity.

With $\varphi = 60°$, the flow starts to deviate upward more rapidly, causing partial bypassing of the heat sinks. The jet loses its attachment to the inlet-facing walls, while the airflow along the top horizontal surfaces weakens. Circulation inside the micro-cavity becomes less pronounced, resulting in a drop in Wall-Resolved heat transfer performance.

Beyond $\varphi = 70°$, a dominant central vortex emerges and occupies most of the cavity volume. The air is redirected upward before effectively reaching the active surfaces, leaving the heat sinks partially isolated from the main flow. Consequently, the micro-cavity region becomes nearly stagnant, and overall cooling efficiency declines sharply.

For the highest inclination **($\varphi = 80°$)**, this trend intensifies. The inflow is almost entirely redirected toward the outlet, with minimal interaction with either the heat-sink surfaces or the vertical walls. The airflow no longer penetrates the micro-cavity, leading to severe thermal stratification and inefficient heat removal.

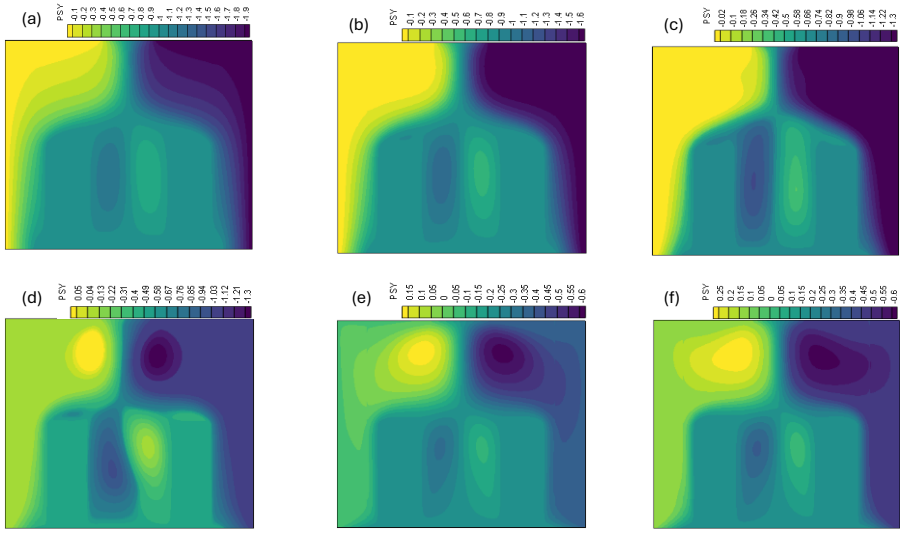

Fig.2. Streamline patterns for K = 50% and different inlet inclination angles (φ)[(a) φ = 0°, (b) φ = 30°, (c) φ = 45°, (d) φ = 60°, (e) φ = 70°, (f) φ = 80°.

Figure 3 presents the isotherm distributions for $K = 50\%$, revealing how the inlet inclination φ governs thermal behavior across three critical regions the heat-sink top surfaces, the inlet-facing vertical walls, and the inter-block micro-cavity. For $\varphi = 0°$, tightly packed isotherms over the horizontal faces indicate efficient heat removal, while wider spacing along the inlet-facing walls and within the micro-cavity signals weak jet interaction and localized heat buildup; the inlet-facing vertical walls are nevertheless well ventilated as the jet impinges and rises along them under combined forced and buoyant effects. In general, tilting the fresh- air jet disrupts the boundary layer along the vertical walls, and this disruption intensifies with increasing inclination; moreover, the upper part of the cavity becomes progressively less ventilated, degrading overall cooling uniformity**.** With $\varphi = 30°$, the isotherms bend toward the sidewalls, yielding modest improvements in wall cooling and steeper gradients in the micro-cavity, consistent with enhanced penetration albeit with some asymmetry. At $\varphi = 45°$, the field is most structured and efficient: sharp, well-distributed gradients span the top faces, vertical inlet walls, and the micro-cavity, marking an effective synergy between forced and buoyant convection for $K = 50\%$. Increasing to $\varphi = 60°$lifts the isotherms toward the upper cavity, indicating less efficient hot-air extraction; while some advection persists over the top faces, ventilation of the micro-cavity and vertical walls declines. At $\varphi = 70°$, stratification intensifies as isotherms recede from the heat sinks and gradients collapse near the micro- cavity and sidewalls, pointing to inefficient extraction and potential hot spots. For the most inclined case, $\varphi = 80°$, the isotherms concentrate almost entirely in the upper region; the inflow detaches from the dissipators, interaction with all key surfaces becomes negligible especially in the micro-cavity and pronounced thermal accumulation ensues, with a marked deterioration of overall cooling performance.

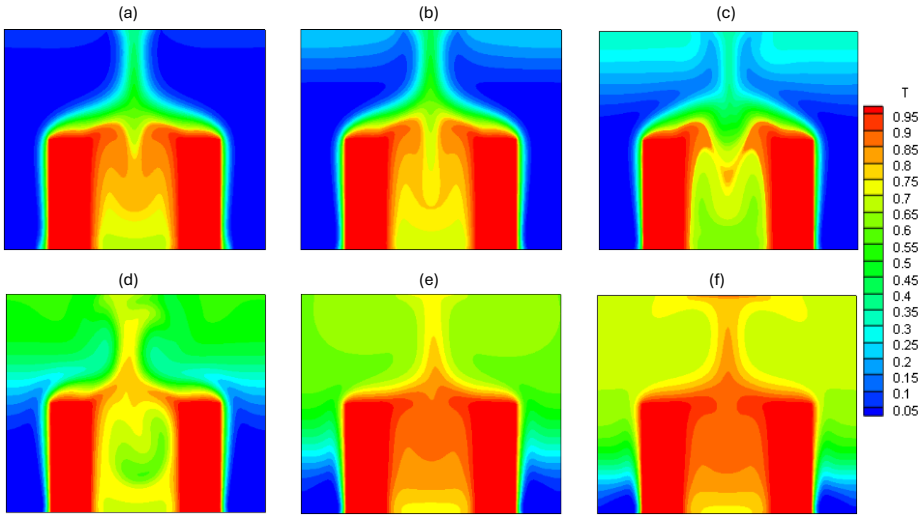

Fig. 3. Isotherm distributions for K = 50% and different inlet inclination angles (φ)[(a) φ = 0°, (b) φ = 30°, (c) φ = 45°, (d) φ = 60°, (e) φ = 70°, (f) φ = 80°

Table.3 Comparison of Flow Behavior and Cooling Efficiency for Different Inlet Inclination Angles

φ°	Jet/ structures	Vertical walls	Top surfaces	Micro-cavity	Mixing / Recirc.	Thermal out come	Overall
0°	Impingement + upwash	Well-washed	Strong impingement	Quasi-stagnant	Weak	Non-uniform; hot spots	Moderate
30°	Inclined jet; corner cells	Good contact	Good coverage	Partial; symmetric	Moderate	Improved uniformity	Good
45°	Dual cells; full coverage	Very good	Very good	Strong penetration	Strong	Uniform; efficient	**Optimal**
60°	Early lift; bypass	Detachment onset	Reduced wash	Weak circulation	Weakened	Degraded extraction	Fair-poor
70°	Central vortex	Poor wash	Poor coverage	Near-stagnant	Limited	Stratifications; hot zones	Low
80°	Outlet-directed jet	Minimal	Minimal	Stagnant	Negligible	Severe accumulation	Very low

3.2 Heat transfer analysis

The variations of the global and wall-resolved Nusselt numbers with the inlet inclination angle, presented in Table 4, highlight the complex interplay between flow redistribution and thermal efficiency for $K = 50\%$. The global Nusselt number Nu_g^m increases from 33.18 at 0° to a peak of 37.81 at 45°, before slightly decreasing at 60° and then dropping more significantly at higher angles, reaching 28.00 at 80°. This behavior indicates that moderate inclination enhances the penetration and distribution of the flow, while excessive tilting reduces its effectiveness due to premature flow deviation toward the outlet.

The vertical wall follows a similar trend, with Nu_{g-in}^m increasing from 12.15 at 0° to a maximum of 13.80 at 45°, reflecting improved shear and boundary layer thinning as the jet progressively aligns with the wall. Beyond this angle, the heat transfer deteriorates, dropping to 10.01 at 80°, due to reduced wall interaction and partial jet detachment.

The horizontal surfaces exhibit a comparable evolution, with Nu_{g-h}^m rising from 3.55 to a maximum of 4.16 at 60°, followed by a decline at higher angles. This indicates that moderate inclination promotes tangential advection above the surfaces, while excessive inclination causes the flow to bypass the heat sinks, reducing residence time and heat exchange.

In contrast, the micro-cavity reaches its optimal convective performance at 45°, with Nu_{g-m-c}^m=1.10, where symmetric recirculation zones enhance fluid renewal between the fins. For higher angles, these recirculations weaken, leading to increased stagnation and a gradual decrease in heat transfer.

Overall, although a slight enhancement of horizontal heat transfer is observed at 60°, the best global and most thermally balanced configuration is achieved at 45°. At this angle, the flow structure ensures an optimal compromise between wall interaction, cavity ventilation, and uniform heat removal, which is essential for preventing localized overheating.

Table.4 Global and Wall-Resolved Nusselt Numbers for Different Inlet Inclination Angles (K = 50%)

$\varphi°/_{Nu}$	0°	30°	45°	60°	70°	80°
Global	33.18	36.62	37.81	37.700	31.75	28.00
Vertical Wall	12.15	13.46	13.80	13.710	11.82	10.01
Horizontal Wall	3.55	3.85	4.00	4.160	3.20	3.13
Micro-cavity	0.89	1.00	1.100	0.973	0.87	0.86

4 Conclusion

This study presents an original and rigorous framework for thermal management optimization based on the Cascaded Lattice Boltzmann Method (CLBM) applied to a periodic cavity with inclined air injection. The results clearly demonstrate that controlling the inlet inclination angle is an effective geometric strategy to simultaneously enhance thermal performance and energy efficiency. The optimal configuration identified at $\varphi = 45°$ yields a global Nusselt gain of +14.00%, along with substantial local improvements: +17.20% on the horizontal surfaces (top of the heat sinks), +23.60% within the micro-cavity (between heat sink), and +15.29% along the vertical wall. Physically, the formation of two stable convection cells at this inclination thins the boundary layers, enhances fluid

mixing, and suppresses hot spots, leading to a lower thermal resistance and a potential reduction in fan power or air flow demand for equivalent cooling capacity. Constant airflow, it also contributes to a reduction in component junction temperature, thus improving energy efficiency, reliability, and lifespan of electronic systems. These results highlight the scientific and practical significance of the present work, providing a geometry-driven cooling optimization strategy that delivers measurable performance gains across all active surfaces particularly the horizontal and micro-cavity regions offering a robust pathway toward compact, energy-efficient, and thermally reliable electronic architectures.

References

1. A. Meskini, M. Najam, M. El Alami, Convective mixed heat transfer in a square cavity with heated rectangular blocks submitted to a vertical forced flow, J. FDMP, 7(1), 97–110 (2011). DOI:10.3970/fdmp.2011.007.097.
2. M. Najam, A. Amahmid, M. Hasnaoui, M. El Alami, Unsteady mixed convection in a horizontal channel with rectangular blocks periodically distributed on its lower wall, Int. J. Heat Fluid Flow, 24(5), 726–735 (2003). DOI:10.1016/S0142-727X(03)00063-8.
3. H. Faraji, M. Teggar, A. Arshad, M. Arıcı, E.M. Berra, K. Choukairy, Lattice Boltzmann simulation of natural convection heat transfer phenomenon for thermal management of multiple electronic components, Therm. Sci. Eng. Prog., 45, 102126 (2023). DOI: 10.1016/j.tsep.2023.102126.
4. M. Mliki, M. Ferhi, M.A. Abbassi, Numerical study of MHD mixed convection of nanofluid flow in a double lid convergent cavity, Acta Mech. Autom., 19(2), 232–242 (2025). DOI:10.2478/ama-2025-0029.
5. R. Hidki, L. El Moutaouakil, M. Boukendil, Z. Charqui, Z. Zrikem, A. Abdelbaki, Impact of Cu–Al2O3/water hybrid nanofluid on natural convection inside a square cavity with two heat-generating bodies, Mater. Today, Proc., 72, 3749–3756 (2023). DOI: 10.1016/j.matpr.2022.09.292.
6. Y. Ma, R. Mohebbi, M.M. Rashidi, Z. Yang, Simulation of nanofluid natural convection in a U-shaped cavity equipped with a heating obstacle: Effect of cavity aspect ratio, J. Taiwan Inst. Chem. Eng., 93, 263–276 (2018). DOI: 10.1016/j.jtice.2018.07.026.
7. F. Selimefendigil, H.F. Öztop, Natural convection and entropy generation of nanofluid-filled cavity having different shaped obstacles under the influence of magnetic field and internal heat generation, J. Taiwan Inst. Chem. Eng., 56, 42–56 (2015). DOI: 10.1016/j.jtice.2015.04.018.
8. A.S. Gawas, D.V. Patil, Natural convection heat transfer with anisotropic thermal diffusion for tilted two-dimensional cavities, Int. J. Heat Mass Transf., 194, 123000 (2022). DOI: 10.1016/j.ijheatmasstransfer.2022.123000.
9. S.D. Farahani, A.D. Farahani, H.F. Öztop, Natural convection in a rectangular tall cavity in the presence of an oscillating and rotating cylinder, Colloids Surf. A Physicochem. Eng. Asp., 647, 129027 (2022). DOI: 10.1016/j.colsurfa.2022.129027.
10. D. Das, M. Roy, T. Basak, Studies on natural convection within enclosures of various (non-square) shapes: A review, Int. J. Heat Mass Transf., 106, 356–406 (2017). DOI: 10.1016/j.ijheatmasstransfer.2016.08.034.
11. F.Z. Laktaoui Amine, M. El Alami, E. Semma, H. Faraji, A. Gounni, A. Mourid, Advanced numerical analysis of heat transfer in medium and large-scale heat sinks using Cascaded Lattice Boltzmann Method, Appl. Sci., 15(13), 7205 (2025). DOI:10.3390/app15137205.
12. F.Z. Laktaoui Amine, E.M. Berra, H. Faraji, M. El Alami, E. Semma, A. Anflous, Height-sensitive mixed convection in confined cavities: Passive cooling enhancement using CLBM in the transitional-to-turbulent regime, Heat Transfer, in press (2025).

DOI:10.1002/htj.70245.
13. G. de Vahl Davis, Natural convection of air in a square cavity: A benchmark numerical solution, Int. J. Numer. Methods Fluids, 3(3), 249–264 (1983). DOI:10.1002/fld.1650030305.